Evidence from detrital chrome spinel chemistry for a Paleo-Tethyan intra-oceanic island-arc provenance recorded in Triassic sandstones of the Nakhlak Group, Central Iran

Seyyedeh Halimeh Hashemi Azizi[a,b,*], Payman Rezaee[a], Mahdi Jafarzadeh[c], Guido Meinhold[b,d], Seyyed Reza Moussavi Harami[d], Mehdi Masoodi[a]

[a] Department of Geology, Faculty of Sciences, 3995 University of Hormozgan, Bandar Abbas, Iran

[b] Abteilung Sedimentologie / Umweltgeologie, Geowissenschaftliches Zentrum Göttingen, Universität Göttingen, Goldschmidtstraße 3, 37077 Göttingen, Germany

[c] Faculty of Geosciences, 3619995161 Shahrood University of Technology, Shahroud, Iran

[d] School of Geography, Geology and the Environment, Keele University, Keele, Staffordshire, ST5 5BG, UK

[e] Department of Geology, Faculty of Sciences, 9177948974 Ferdowsi University of Mashhad, Mashhad, Iran

* Corresponding author: Department of Geology, Faculty of Sciences, 3995 University of Hormozgan, Bandar Abbas, Iran.

Tel.: +98 935 519 6994.

E-mail address: hashemi.azizi@gmail.com (S.H. Hashemi Azizi)

Abstract

Detrital chrome spinel (Cr-spinel) is for the first time described from the Nakhlak Group, which is a distinctive Triassic (Late Olenekian–?Early Carnian) sedimentary succession in Central Iran. Previously published data from the Nakhlak Group suggest deposition along an active margin during the Triassic and Eurasian affinity. Presently, the Nakhlak Group is located in the northwestern region of the Central-East Iranian Microcontinent, a major segment of the Cimmerian block. The Nakhlak region is believed to have been dislocated from its prior position at the Turan Plate from the southern Eurasian active margin after deposition in Triassic time. Almost all of the analysed detrital Cr-spinels have high Cr-numbers (0.6–0.85), variable Mg-numbers (0.33–0.78), and low Fe^{3+} (<0.25), Al_2O_3 (<20 wt%) and TiO_2 (<0.4 wt%) contents, suggesting a magmatic source for the Cr-spinels formed both within oceanic (mainly harzburgitic) mantle and in a supra-subduction zone (SSZ) tectonic setting. The data suggest that mafic–ultramafic rock assemblages with SSZ signatures were generated in the Paleo-Tethyan realm before their obduction as an ophiolite. By comparing data from the present study with results from previous work on the Triassic in Central Iran it is evident that Paleo-Tethyan ophiolites of intra-oceanic island-arc (IOIA) origin supplied detrital material to the Nakhlak Group at the southern margin of Eurasia during pre- to syn-Eocimmerian tectonics in the Triassic.

Keywords: Sediment provenance; detrital chrome spinel; Triassic; Nakhlak Group; Central Iran; Paleo-Tethys

Research highlights

► Cr-spinel is for the first time reported from the Triassic of Iran.

► The Cr-spinels are mainly high Cr-type derived from podiform chromitites.

► The chromitites probably formed in an intra-oceanic island-arc setting during the Paleozoic.

► Ophiolitic rocks along Eurasia's southern margin supplied Cr-spinels to the Triassic sediments.

1. Introduction

Detrital Cr-spinel is a reliable petrogenetic and provenance indicator (e.g., Pober and Faupl, 1988; Cookenboo et al., 1997; Lužar-Oberiter et al., 2009; Caracciolo et al., 2015; Baxter et al., 2016). Because of its chemical durability and mechanical stability, its compositional signature after burial in sedimentary strata is preserved, in contrast with olivine and most other mafic minerals, which are altered rapidly at near surface conditions (e.g., Morton and Hallsworth, 1999, and references therein), and thus Cr-spinel is often the only remnant of those tectonic slabs of oceanic crust involved into orogenic collision zones. In addition, Cr-spinel is a sensitive indicator of melt composition and pressure of crystallization (e.g., Dick and Bullen, 1984; Barnes and Roeder, 2001; Kamenetsky et al., 2001), because Cr-spinel is an early forming phase which precipitates before the magma composition is affected by crystallization of silicate minerals (Zhou and Robinson, 1994).

Mafic–ultramafic rocks of ophiolite complexes are the main source for detrital Cr-spinel (Mosier et al., 2012). Paleozoic ophiolites, interpreted as remnants of the Paleo-Tethys, are preserved in southwestern Eurasia (e.g., Turkey, Caucasus, Iran, Turkmenistan, and Afghanistan). In northern Iran, from west to east, remnants of Paleo-Tethys ophiolites include the Takab ophiolite, Rasht ophiolite, South Caspian Sea Basin ophiolite, Aghdarband ophiolite, and Mashhad ophiolite (Fig. 1a). Paleozoic ophiolites are also found in the NW region of the Central-East Iranian Microcontinent (CEIM), which hosts the Anarak, Jandaq, Bayazeh and Posht-e-Badam ophiolites (Fig. 1a). They are affiliated to the northern Iranian

Paleo-Tethys suture zone and related Variscan terranes of the Turan Plate (e.g., Bagheri and Stampfli, 2008; Zanchi et al., 2015). The western part of the CEIM is thought to be dislocated from its primary formation site, which was located close to the Aghdarband region (NE Iran) somewhere at the Turan Plate (southern Eurasia). This region attached to the Cimmerian block following the Cimmerian–Eurasian collision, then detached from Eurasia and transferred to central Iran by a counterclockwise rotation, which is supported by paleomagnetic data (Davoudzadeh et al., 1981; Soffel and Forster, 1984; Soffel et al., 1996; Alavi et al., 1997; Mattei et al., 2012, 2015). Based on the structural interpretation of high-resolution aeromagnetic and radiometric data in central Iran, anticlockwise rotation of the CEIM is confirmed by widespread dextral shearing during the Late Triassic–Early Cretaceous (Basson et al., 2016).

In the western part of the CEIM, to the north of the Anarak ophiolite, Triassic sedimentary rocks of the Nakhlak Group crop out in the Nakhlak Mountain (Fig. 1b and c). These rocks are distinctive and unique in Central Iran because they are similar to Triassic successions in NE Iran (e.g., Alavi et al., 1997; Vaziri, 2001), i.e. to the north of the Northern Iranian Paleo-Tethys suture zone. Constraining the provenance of the Nakhlak Group is important for geodynamic reconstructions of the Paleo-Tethyan realm. Here we report for the first time the occurrence of detrital Cr-spinel grains in the Nakhlak Group sediments and present mineral geochemistry to decipher their source. The new data are the first evidence for sediment supply from Paleo-Tethyan ophiolites of intra-oceanic island-arc origin during pre- to syn-Eocimmerian convergence in Iran.

(Figure 1)

2. Geological setting

2.1. Major structural units of Iran

Stöcklin (1968) subdivided Iran into nine major structural zones (Fig. 1a), which differ in their structural history and tectonic style. The *Plain of Shatt-al-Arab* is structurally part of the Arabian platform. The *Zagros Fold Belt* comprises a continuous, conformable marine sequence, ranging in age from Lower Mesozoic to Neogene. The folded belt passes northeastward without a sharp boundary into a narrow zone of thrusting, the *Zagros Thrust Zone*, bounded on the northeast by the main Zagros thrust line. The *Sanandaj–Sirjan Ranges* are the ranges that follow northeast of the main Zagros thrust. The structural zone of *Central Iran* comprises a roughly triangular area limited by the Lut block on the east, the Alborz Mountains on the north, and the Sanandaj–Sirjan Ranges on the southwest. Within Central Iran, the area termed by Stöcklin (1968) "eastern Central Iran", later changed to Central-East Iranian Microcontinent (Takin, 1972), can be distinguished as a special subzone. This area is bordered by the Great Kavir Fault in the north, the Nain–Baft Fault in the west and southwest, and by the Harirud Fault in the east (Davoudzadeh et al., 1981). The *Alborz Mountain* is a well-defined mountain range in the north of Iran. The *Kopeh Dagh Range* occupies the border region between Iran and Turkmenistan. The *Lut Block* is an irregularly outlined, essentially N–S trending, rigid mass smoothly surrounded by the ranges of Central and East Iran. The *Makran and East Iranian Ranges* are much more closely related to the Baluchistan–Indus Ranges of Pakistan than to the rest of Iran. The reader is referred to Stöcklin (1968), Takin (1972), Berberian (1981), Alavi (1991) and Nogole-Sadat (1993) for more information about the major structural zones of Iran.

Additionally, the presence of several ophiolitic belts may represent the opening and closure of many oceanic basins and the complex geological history of Iran. One of the main structural units is the Central-East Iranian Microcontinent (CEIM). The study area is located in the NW part of the CEIM (Fig. 1a). Here the Anarak Metamorphic Complex (AMC) crops out including the Paleozoic Anarak metamorphic rocks and associated ophiolite (Sharkovski

et al., 1984; Bagheri and Stampfli, 2008; Buchs et al., 2013; Torabi, 2013; Shafaii Moghadam and Stern, 2014). The ophiolite is mainly composed of (i) serpentinite to serpentinitic peridotite lenses that in few places have been intruded by gabbroic–basaltic bodies and dykes as well as trondhjemite (plagiogranite) and (ii) pillow lavas (OIB type) overlain by rhyolites (Sharkovski et al., 1984; Bagheri and Stampfli, 2008; Shafaii Moghadam and Stern, 2014). The nearest other Paleozoic ophiolites occur at Jandaq to the NE and at Bayazeh to the SE (Torabi et al., 2011; Nosouhian et al., 2014a) (Fig. 1a). The Jandaq ophiolite is composed of metamorphosed peridotite and serpentinized peridotite (mainly lherzolite and minor harzburgite), gabbro, amphibolite, rodingite and listwaenite (Torabi et al., 2011). Mesozoic granite intrusions crosscut the Jandaq ophiolite (Torabi et al., 2011). The Bayazeh ophiolite is mainly composed metamorphosed serpentinite and serpentinized peridotite (mainly harzburgite), gabbro, ultramafic dykes, picrite, and listwaenite (Nosouhian et al., 2014a). These ophiolites represent remnants of the Paleo-Tethys (Bagheri and Stampfli, 2008; Zanchi et al., 2009a, b; Buchs et al., 2013). Zanchi et al. (2015) suggest that the AMC belongs to a Variscan accretionary wedge developed along the southern Eurasian margin before the Cimmerian parts of Iran collided with that. Bagheri and Stampfli (2008) have established two low-grade metamorphic units (Doshakh accretionary wedge and Bayazeh Flysch) of Permian to Triassic age further to the south of Anarak, along with the Paleo-Tethys suture zone. These units also record the progressive closure of the Paleo-Tethys during the Cimmerian collision.

The whole region between Anarak and Jandaq further north has been considered as part of a large allochthonous block, which was probably located in a very different tectonic position (Bagheri and Stampfli, 2008; Zanchi et al., 2009a, b; Buchs et al., 2013; Zanchi et al., 2015). In fact, it suggested that the AMC has once been connected to the Upper Paleozoic units of NE Iran, Fariman Complex and Binalood units (Zanchi et al., 2015).

The CEIM appears to have been rotated in an anticlockwise sense and is surrounded by an Upper Cretaceous to Lower Eocene ophiolite and ophiolitic mélange (Fig. 1a). It is very

156 wide in the Sabzevar–Torbat area, considerably narrower at Nain, and locally reduced to an
157 exposed width of only few hundred meters southwest of the Shirkuh Microblock (Stöcklin,
158 1968).
159
160 *2.-2. Geology of the Nakhlak Group*
161
162 The study area is located to the north of the Anarak (Fig. 1a and b). It comprises the Nakhlak
163 Mountain where the Nakhlak Group is exposed (Figs 1c and 2). This group includes three
164 formations (from oldest to youngest) (e.g., Davoudzadeh and Seyed-Emami, 1972; Alavi et
165 al., 1997; Vaziri, 2001; Balini et al., 2009; and own observations): the Alam, Baqoroq, and
166 Ashin formations. The Alam Formation was deposited in the Upper Olenekian–Anisian as
167 constrained by bivalves and ammonoids (Tozer, 1972; Vaziri and Fürsich, 2007; Balini et al.,
168 2009) and conodonts (Balini et al., 2009). The Alam Formation is a 1060-m-thick mixed
169 volcanic siliciclastic and calcareous succession (Fig. 2a–c) which starts with volcaniclastic
170 beds, followed by ooid-bearing calcareous massive layers and fossiliferous limestones,
171 deposited in an agitated shallow shelf depositional environment. The Alam Formation
172 continues into a thick sequence of thin sandy-, silty-, and calcareous ammonoid-bearing beds,
173 representing different parts of the Bouma sequence (Bouma, 1962), deposited by turbidity
174 currents in the deeper parts of the basin (Fig. 2b). In the middle part of the Alam Formation,
175 there is a pseudo-nodular fossiliferous limestone sequence, which followed by thick
176 calcareous shale beds approaching the top of the formation. Detrital mode analysis revealed
177 that most of the sandstone samples from the Alam Formation include dominantly volcanic
178 detritus mainly represented by lithic fragments and single phenocrysts such as volcanic quartz
179 grains and feldspars (Fig. 3a and b). The average quartz–feldspar–lithic fragment ratio is
180 $Qt_{21.6}$:$F_{38.7}$:$L_{39.7}$ (S.H. Hashemi Azizi, unpublished data).

The Baqoroq Formation, which lies with an erosive contact above the Alam Formation, is barren from any types of fossils which leads to an age assignment of Late Anisian–?Early Ladinian considering its stratigraphic position between the Alam and Ashin formations (Davoudzadeh and Seyed-Emami, 1972; Balini et al., 2009). This 1294-m-thick formation starts with a conglomerate bed, which consists of ooid grainstone pebbles, probably originated from the Alam Formation, and continuous into a red massive conglomeratic sequence (Fig. 2a and c–e). Generally, the Baqoroq Formation can be subdivided into two main bodies of conglomerates. The first body of massive conglomerate beds comprises first-cycle sedimentary and volcanic material as well as some recycled metamorphic basement such as polycrystalline quartz. The second body of massive conglomerate beds is composed of less sedimentary and volcanic material and is chiefly composed of low-grade metamorphic detritus. The Baqoroq Formation shows a red color and sedimentary structures (e.g., massive gravel matrix- and clast-supported, horizontal bedding, imbrication, and trough cross-beds) demonstrate a gravel-bed fluvial depositional environment (Miall, 2006). Detrital mode analysis showed a hybrid composition for the Baqoroq Formation including low-grade metamorphic and volcanic as well as sedimentary detritus (Fig. 3c–e). The average quartz–feldspar–lithic fragment ratio is Qt_{45}:$F_{19.7}$:$L_{35.3}$ (S.H. Hashemi Azizi, unpublished data).

The Baqoroq Formation is conformably overlain by the 364-m-thick Ashin Formation, which is dominated by shale beds intercalated with thin sandstone, calcareous siltstone and fossiliferous limestone (Fig. 2f and g). The upper part of this formation has been tectonically truncated. Limestone and shale beds contain fossil remains such as ammonoids, bivalves, and crinoids suggesting a Ladinian–?Early Carnian age (Tozer, 1972; Vaziri and Fürsich, 2007; Balini et al., 2009). Sedimentary structures characteristic for Bouma sequences (Bouma, 1962) and *Nereites* ichnofacies suggest that the Ashin Formation was deposited by distal turbidity currents. Modal analysis showed the Ashin Formation sandstones contain chiefly K-

206 feldspar and volcanic detritus as well as some fossil fragments (Fig. 3f). The average quartz–
207 feldspar–lithic fragment ratio is $Qt_{35}:F_{46.5}:L_{18.5}$ (S.H. Hashemi Azizi, unpublished data).
208
209 (Figure 2)
210 (Figure 3)
211
212 3. Materials and methods
213
214 Samples were taken from fine- to medium-grained sandstone beds, crushed and dry-
215 sieved to obtain the 63–125 μm fractions. Carbonate was removed by 5% cold acetic acid
216 treatment. Heavy fractions were separated by immersion in heavy liquid (sodium
217 polytungstate, $\rho = 2.85$ g cm^{-3}). Cr-spinel selection from the heavy fractions was achieved by
218 handpicking under a binocular microscope. Cr-spinel grains were fixed in an epoxy resin
219 mount and polished (see Appendix A). The grains were analyzed with a JEOL JXA 8900 RL
220 electron probe microanalyzer (EPMA) equipped with five wavelength dispersive
221 spectrometers at the University of Göttingen (Department of Geochemistry, Geoscience
222 Center). Conditions included an accelerating voltage of 20 kV and a beam current of 20 nA.
223 The counting times were 15 s for Mg, Al, Si, and Fe, and 30 s for Cr, Ti, Mn, V, Ni, and Zn.
224 Matrix correction was performed using the Phi-rho-Z procedure. Ferrous and ferric Fe in Cr-
225 spinel were calculated from raw analyses assuming spinel stoichiometry. Data evaluation and
226 calculation of atomic ratios followed standard procedures (Barnes and Roeder, 2001).
227 Representative Cr-spinel analyses are given in Table 1. The full dataset is provided as
228 Supplementary material (see Appendix A).
229
230 (Table 1)
231 4. Results

In total, we analyzed 250 Cr-spinel grains from six sandstone samples taken from the Alam, Baqoroq, and Ashin formations (two samples per formation) (Fig. 1c). Representative photomicrographs taken from Cr-spinel samples of the Alam, Baqoroq, and Ashin formations are provided as Supplementary material (see Appendix A). The mineral chemical results for all samples are illustrated in Figs. 4–6.

4.1. Alam Formation

In total 99 Cr-spinel grains were analyzed from the Alam Formation (GPS coordinates of sample localities: sample AN4H: 33°32′40.21″ N, 53°48′39.83″ E; sample AN278H: 33°33′41.75″ N, 53°47′49.33″ E). Cr-number [Cr# = Cr/(Cr + Al)] values of the analyzed Cr-spinels range from 0.62 to 0.82 (average of 0.75), mostly (59%) between 0.70 and 0.79, with two grains containing high Cr# values (0.89 and 0.93). Mg-number [Mg# = Mg/(Mg + Fe^{2+})] values range from 0.43 to 0.77 (average of 0.69), with limited Mg:Fe variations. Fe^{3+} values are consistently low. The maximum Fe^{3+}/(Fe^{3+} + Cr + Al) value in the Alam Formation spinels is 0.07. TiO_2 values range between 0.09 and 0.37 wt% (average of 0.21) with 33% having TiO_2 concentrations above 0.2 wt%. A ternary plot of Cr–Al–Fe^{3+} (Fig. 4) is commonly used for discriminating Alpine-type peridotites from Alaskan-type and stratiform peridotite complexes. In Alpine-type peridotites, Cr increases with increasing Fe^{3+}, but Fe^{3+} concentrations overall remain quite low. The most significant chemical variation of spinel in abyssal spinel-peridotites is a large reciprocal variation of Cr and Al. Those abyssal peridotites with spinel compositions at the high-chrome end of the spinel range are generally harzburgites (Dick and Bullen, 1984). Spinel compositions from the Alam Formation plot at the high-Cr end; the Cr concentration increases with increasing Fe^{3+}, but Fe^{3+} remains low (Fig. 4a), consistent with an Alpine-type peridotite origin. Because Cr-spinels of abyssal

peridotites are limited by upper Cr# values of 0.6, whereas the values of spinels of Alpine-type peridotites reach up to 0.85 (Dick and Bullen, 1984), Cr-spinels from the Alam Formation are more likely to have originated from Alpine-type peridotites. According to the Dick and Bullen (1984) peridotite classification scheme, Alam Formation spinels fit to type III peridotites and associated volcanics (Cr# >0.6 and very low Ti), which are found to be related to island arc/back-arc systems. In the Cr# versus Mg# diagram (Fig. 4d) all data fall within the podiform chromitites field except four grains fall in the area participated by harzburgites defined by Pober and Faupl (1988). Spinels from Alam Formation are highly magnesian, and Fe^{2+}:Mg ratios are almost constant (0.29–0.83) which agrees with Dickey (1975) assertion about constant Fe^{2+}:Mg ratio in chromites from podiform deposits. In the Fe^{2+}/Fe^{3+} and TiO_2 versus Al_2O_3 discrimination diagrams proposed by Kamenetsky et al. (2001) most of the data fall in the field of arc rocks and volcanic spinels, some spinel grains lie in the field of the supra-subduction zone (SSZ) peridotites (Fig. 5). In the TiO_2 versus Cr# diagram most of the high-Cr chromites plot in the boninitic field (Fig. 6a).

4.2. Baqoroq Formation

In total 51 Cr-spinel grains were analyzed from Baqoroq Formation (GPS coordinates of sample localities: sample B2H: 33°33′45.67″ N, 53°47′50.97″ E; sample B11H: 33°33′44.88″ N, 53°48′26.07″ E). Generally, high-Cr# spinels from podiform chromitites predominate in Baqoroq Formation (Fig. 4e). Sample BH2 contains 85% spinels with Cr# 0.6–0.8. Two grains are relatively high in Al^{3+} (0.99 and 1.15) with Cr# as low as 0.32 and 0.41. Sample BH11 contains spinels with Cr# values between 0.32 and 0.82 and Mg# values between 0.33 and 0.74, with Mg concentration generally decreasing as Fe increases. The maximum $Fe^{3+}/(Fe^{3+} + Cr + Al)$ in the analyzed spinels is 0.13. TiO_2 values range between 0.01 and 0.71 wt% (average of 0.17), with 22% having TiO_2 concentrations above 0.2 wt%.

Fig. 4b shows Alpine-type peridotite as possible source rocks, except two grains that contain low Cr and high Al. According to the Dick and Bullen (1984) peridotite classification scheme, Baqoroq Formation spinels fit all three types of peridotites. In the Cr# versus Mg# diagram (Fig. 4e), most of the data fall in the podiform chromitites field, some grains lie in the harzburgites field and one grain plots in the cumulates field (Pober and Faupl, 1988). On the Fe^{2+}/Fe^{3+} and TiO_2 versus Al_2O_3 diagrams, most of the spinels fall in the field of arc rocks and volcanic spinels, while some spinels plot in the field of SSZ peridotites and MORB (Fig. 5b and e). In a TiO_2 versus Cr# diagram most of the high-Cr chromites plot in the boninitic field and two grains plot in the MORB field (Fig. 6b).

The data clearly illustrate that Cr-spinels from the Baqoroq Formation slightly differ from Cr-spinels of the two other formations of the Nakhlak Group. The slightly more variable compositions in the Baqoroq Formation are consistent with exposure of additional source rocks in basically the same source area. A similar conclusion that source rocks became more varied through time is evident from the detrital modes of the sandstones (Balini et al., 2009; S.H. Hashemi Azizi, unpublished data). In fact, more feldspatholithic and quartzofeldspathic sandstones in the Alam Formation transition into more lithoquartzose and feldspathoquartzose sandstones in the Baqoroq Formation; furthermore, there is less volcanic input in the Baqoroq Formation compared with the Alam Formation. As a matter of fact, there is a conspicuous transition from volcanic to metamorphic detritus within the Baqoroq Formation; volcanic detritus derived from active arcs or eroded inactive arcs plus quartz-schist lithic fragments are plentiful in the lower part of the formation while volcanic detritus is absent in the upper part that is chiefly composed of quartz-schist and quartz-muscovite-schist. Thus, an overall comparison of the Alam and Baqoroq formations confirms obvious changes in lithology like the remarkable increase of the abundance of polycrystalline quartz, a considerable decrease of volcanic input, and the presence of low-grade metamorphic detritus in the Baqoroq Formation. A decrease in the abundance of volcanic-derived material is probably related to a

quiescence phase in arc activity, which supplied volcanic material in the Alam Formation. The availability of metamorphic-basement-derived components in the Baqoroq Formation may be related to different criteria such as a) Eustatic sea level drop during the late Anisian (Ogg et al., 2016); b) Uplifted basement during the early Ladinian by pre-Cimmerian tectonics.

4.3. Ashin Formation

In total 100 Cr-spinel grains were analyzed from the Ashin Formation (GPS coordinates of sample localities: sample AS1H: 33°34′18.81″ N, 53°48′13.79″ E; sample AS107H: 33°34′16.78″ N, 53°48′46.29″ E). The Cr-spinels from the Ashin Formation show a range of Cr# between 0.62 and 0.85 (average of 0.77) and Mg# values between 0.42 and 0.78 (average of 0.68), with limited Mg:Fe variations. The maximum $Fe^{3+}/(Fe^{3+} + Cr + Al)$ in Ashin Formation spinels is 0.07. TiO_2 values range between 0.04 and 0.39 wt% (average of 0.19), with 26% having TiO_2 concentrations above 0.2 wt%. Fig. 4c depicts Alpine-type peridotite for Ashin Formation spinels. All data cluster in the podiform chromitites field (Fig. 4f). On the Fe^{2+}/Fe^{3+} and TiO_2 versus Al_2O_3 diagrams (Fig. 5c and f) most of the data fall in the field of arc rocks and volcanic spinels, while some spinel grains lie in the field of SSZ peridotites. In a TiO_2 versus Cr# diagram most of the high-Cr chromites plot in the boninitic field and one grain plots in the MORB field (Fig. 6c). Overall, spinel compositions in Ashin and Alam formations sandstones are similar.

(Figure 4)

(Figure 5)

(Figure 6)

5. Discussion

Electron microprobe data reveal that almost all analyzed detrital Cr-spinel grains from the Nakhlak Group sandstones belong to the magnesiochromite series, which is characterized by having both Cr# and Mg# values >0.5. Podiform chromitites are probably the source for most of these high-Cr grains. Podiform chromitites typically occur as lenticular or pod-shaped bodies, a few meters or tens of meters in length, and most of these may be formed in the upper mantle or in the mantle-crust transition zone in an oceanic arc environment (Dickey, 1975; Zhou and Robinson, 1994; Arai and Yurimoto, 1995; Robinson et al., 1997). High-Cr type chromites generally contain less than 0.4 wt% TiO_2, have high Cr contents (Cr# > 0.6), and are characterized by wider ranges of FeO and MgO than the high-Al series (Dickey, 1975). Chromites from individual podiform chromitite deposits have an almost constant Fe^{2+}/Mg ratio (Dickey, 1975). These chromites are typically crystalized from highly magnesian magmas (boninitic type formed by a high degree of partial melting) and hosted in highly depleted harzburgites (Zhou and Robinson, 1994; Zhou et al., 1994; Robinson et al., 1997). Chromium-rich, Mg-rich chromites are the hallmark of primitive mantle-derived magmas (Barnes and Roeder, 2001). Considering the TiO_2 and Cr# values, Nakhlak Group Cr-spinels resemble spinels found in boninites (Arai, 1992; Pagé and Barnes, 2009) (Fig. 6). About 22–33% of the Cr-spinel grains from the Nakhlak Group have ≥0.2 wt% TiO_2, suggesting that some of the Cr-spinels are likely derived from volcanics. The Baqoroq Formation has least grains (only 22%) containing high TiO_2 while the Alam Formation has most grains (33%) containing high TiO_2.

Geochemical characteristics of the Nakhlak Group spinels suggest podiform chromitites hosted in highly depleted harzburgites as source rocks. According to Robinson et al. (1997) and Zhou et al. (2014), podiform chromites occur primarily in SSZ mantle sections and their chemical compositions can be correlated with the formation in different tectonic

362 settings, especially intra-oceanic island arcs and nascent spreading centers that form in back-
363 arc basins. It is therefore likely that SSZ-influenced mantle material and volcanic arc rocks
364 are the sources of the Cr-spinels in the Nakhlak Group sediments. The SSZ-related magmatic
365 activity and volcanic arc formation were related to intra-oceanic subduction of Paleo-Tethys
366 lithosphere probably at some point between the Devonian and Permian (Fig. 7). Later, likely
367 during the Permian, chromitite-bearing SSZ peridotites were obducted onto the continental
368 Eurasian crust and were eroded into a fore-arc basin during the Triassic (Fig. 7). Balini et al.
369 (2009) in their petrographic study of sandstones and conglomerates of the Nakhlak Group
370 oppose the occurrence of ophiolitic rock fragments (serpentinites) reported by Alavi et al.
371 (1997). Although in the present study, we could not find any ophiolitic rock fragments, we
372 found detrital Cr-spinel grains, which have survived weathering and burial diagenesis. Even
373 so, the heavy mineral assemblage includes plenty of Cr-spinel grains, Nakhlak Group
374 sandstones are barren in ultramafic rock fragments and in fact are dominated by fresh
375 volcanic derived material of felsic–intermediate composition in samples from the Alam and
376 Ashin formations, whereas sandstones of the Baqoroq Formation show a mixed provenance of
377 arc and recycled orogen (Balini et al., 2009; S.H. Hashemi Azizi, unpublished data). The
378 detrital material was not transported over long distances. All of that can be explained by
379 placing the Nakhlak Group depositional system in a fore-arc basin setting where the fresh
380 volcanic material comes from arc volcanic rocks and Cr-spinel grains from both volcanics and
381 the recycling of unstable ultramafic rock fragments from an ophiolite complex (Fig. 7).
382 The nearest ophiolite complexes of Paleozoic age are found in the Jandaq and Anarak
383 regions. Late Paleozoic igneous rocks show clear SSZ (back-arc extension, BABB-like
384 volcanic rocks) geochemical signatures, and preceding formed metabasites show OIB and
385 MORB signatures (e.g., Shafaii Moghadam and Stern, 2014, and references therein). Cr-
386 spinels from the Jandaq peridotites have Cr-numbers (0.46–0.61), Mg-numbers (0.38–0.61)
387 and TiO_2 values (0.00–0.42 wt%) (Torabi et al., 2011) similar to some Cr-spinels found in the

Baqoroq Formation (this study), indicating lherzolitic to harzburgitic sources. Spinel compositions from the Baqoroq Formation are more diverse compared with spinel compositions from the Alam and Ashin formations, which only contain volcanic arc and SSZ originated spinels. Petrological observations (Balini et al., 2009; Zanchi et al., 2009b; S.H. Hashemi Azizi, unpublished data) also confirm that the Baqoroq Formation has a greater diversity in the composition of its components. This indicates that additional source rocks have been exposed in the source area during the time of deposition of the Baqoroq Formation. Metasedimentary (quartz-mica schist) clasts from the Baqoroq Formation are similar to metamorphic components of the Anarak Metamorphic Complex (AMC). Minor parts of the latter are also exposed in the Nakhlak Mountain, but most exposures of the AMC are found to the south of the Nakhlak Mountain (Fig. 1). However, the Jandaq and Anarak ophiolites do not contain chromitites because of inappropriate chemical compositions of mantle peridotite and pyroxenes (low Cr contents) and an insufficient degree of partial melting of mantle rocks (Torabi, 2013). The chemical composition of spinels in Paleozoic ophiolites of NE Iran (Shafaii Moghadam et al., 2015) is also different to those of this study. Considering the lower Cr# (0.61–0.68) and Fe^{+3}# (0.02–0.04) and slightly higher SiO_2 values, the detrital input of Cr-spinels from serpentinites of the Bayazeh ophiolite (Nosouhian et al., 2014b) is also excluded. Although there are many ophiolite bodies in the region that are related to the Paleo-Tethys subduction, those have no potential of being source rocks for the Nakhlak Group spinels. The Cr-spinel-bearing source rocks have probably been eroded completely or buried since the Triassic. Regardless of this, the recognition of detrital Cr-spinel grains in the Triassic Nakhlak Group is important for sediment provenance studies and paleotectonic reconstructions of the Paleo-Tethyan realm in the Middle East.

(Figure 7)

6. Conclusions

Most of the detrital Cr-spinel grains in the Triassic Nakhlak Group display considerably high Cr- and Mg-numbers. An ophiolitic source is suggested which comprises podiform chromitites emplaced in depleted peridotites associated with mafic magma, which developed in a supra-subduction zone and arc setting. The mineral chemical composition of the detrital Cr-spinels is similar in the whole Nakhlak Group, especially in the Alam and Ashin formations, suggesting a uniform source area during the Late Olenekian–?Early Carnian. The Baqoroq Formation contains some spinel grains with slightly different composition, which can be explained by a different input into the same basin, supplied by a source similar to the Anarak and Jandaq ophiolites. The occurrence of detrital Cr-spinel grains in the Nakhlak Group provides (i) evidence for the presence of an intra-oceanic island-arc system within the Paleo-Tethyan realm and (ii) good time constraints on the obduction and erosion history of Paleo-Tethys related ophiolites before the final collision of the Cimmerian blocks with the southern Eurasian margin. At present, however, an exact source area cannot be constrained due to the lack of sufficient Cr-spinel chemical reference data of pre-Mesozoic ophiolites in Iran.

Acknowledgements

The present paper is a part of the first author’s Ph.D. dissertation, which was partially supported by the University of Hormozgan; financial support for the first author's research stay in Germany has been provided by the Ministry of Sciences, Researches, and Technology of the Islamic Republic of Iran. We are grateful to Andreas Kronz for providing access to the electron microprobe. Support by the Geoscience Center Göttingen is gratefully acknowledged. Helpful comments from Alan Baxter on an earlier draft of this manuscript are much appreciated.

Appendix A. Supplementary data

Supplementary data to this article can be found, in the online version, at xxx.

References

Alavi, M., 1991. Sedimentary and structural characteristics of the Paleo-Tethys remnants in northeast Iran. Geological Society of America Bulletin 103, 983–992.

Alavi, M., Vaziri, H., Seyed Emami, K., Lasemi, Y., 1997. The Triassic and associated rocks of the Nakhlak and Aghdarband areas in central and northeastern Iran as remnants of the southern Turanian active continental margin. Geological Society of America Bulletin 109, 1563–1575.

Angiolini, L., Gaetani, M., Muttoni, G., Stephenson, M.H., Zanchi, A., 2007. Tethyan oceanic currents and climate gradients 300 m.y. ago. Geology 35, 1071–1074.

Arai, S., 1992. Chemistry of chromian spinel in volcanic rocks as a potential guide to magma chemistry. Mineralogical Magazine 56, 173–184.

Arai, S., Yurimoto, H., 1995. Possible sub-arc origin of podiform chromitites. Island Arc 4, 104–111.

Bagheri, S., Stampfli, G.M., 2008. The Anarak, Jandaq and Posht-e-Badam metamorphic complexes in Central Iran: new geological data, relationships and tectonic implications. Tectonophysics 451, 123–155.

Balini, M., Nicora, A., Berra, F., Garzanti, F., Levera, M., Mattei, M., Muttoni, M., Zanchi, A., Bollati, I., Larghi, C., Zanchetta, S., Salamati, R., Mossavvari, F., 2009. The Triassic stratigraphic succession of Nakhlak (Central Iran), a record from an active margin. In: Brunet, M.F., Wilmsen, M., Granath, J.W., (Eds.), South Caspian to Central Iran Basins. Geological Society London, Special Publications 312, pp. 287–321.

Barnes, S.J., Roeder, P.L., 2001. The range of spinel compositions in terrestrial mafic and ultramafic rocks. Journal of Petrology 42, 2279–2302.

Basson, I.J., Ravasan, R., Mahdavi, F., Hemmati, Y., Sabzehparvar, M., Masoodi, M., Wooldridge, A., Andrew, J., Doyle, G., King, J., 2016. Structural interpretation of new high-resolution aeromagnetic and radiometric data in Central Iran. Conference Proceedings of SEG 2016: Tethyan Tectonics and Metallogeny, 25–28 September 2016, Çeşme, Turkey.

Baxter, A.T., Aitchison, J.C., Ali, J.R., Sik-Lap Chan, J., Nagi Chan, G.H., 2016. Detrital chrome spinel evidence for a Neotethyan intra-oceanic island arc collision with India in the Paleocene. Journal of Asian Earth Sciences 128, 90–104.

Berberian, M., King, G.C.P., 1981. Towards a paleogeography and tectonic evolution of Iran. Canadian Journal of Earth Sciences 18, 210–265.

Berra, F., Zanchi, A., Angiolini, L., Vachard, D., Vezzoli, G., Zanchetta, S., Bergomi, M., Javadi, H.R., Kouhpeima, M., 2017. The Upper Palaeozoic Godar–e-Siah Complex of Jandaq: Evidence and significance of a north Palaeotethyan succession in Central Iran. Journal of Asian Earth Sciences 138, 272–290.

Bouma, A.H., 1962. Sedimentology of some flysch deposits; a graphic approach to facies interpretation. Elsevier, Amsterdam, 168 pp.

Buchs, D.M., Bagheri, S., Martin, L., Hermann, J., Arculus, R., 2013. Paleozoic to Triassic ocean opening and closure preserved in Central Iran: Constraints from the geochemistry of meta-igneous rocks of the Anarak area. Lithos 172–173, 267–287.

Caracciolo, L., Critelli, S., Cavazza, W., Meinhold, G., von Eynatten, H., Manetti, P., 2015. The Rhodope Zone as a primary sediment source of the southern Thrace basin (NE Greece and NW Turkey): evidence from detrital heavy minerals and implications for central-eastern Mediterranean palaeogeography. International Journal of Earth Sciences 104, 815–832.

491 Cookenboo, H.O., Bustin, R.M., Wilks, K.R., 1997. Detrital chrome spinel compositions used
492 to reconstruct the tectonic setting of provenance: implication for orogeny in the Canadian
493 cordillera. Journal of Sedimentary Research 67, 116–123.
494 Davoudzadeh, M., Seyed-Emami, K., 1972. Stratigraphy of the Triassic Nakhlak Group,
495 Anarak region, Central Iran. Geological Survey of Iran, Report 28, 5–28.
496 Davoudzadeh, M., Soffel, H., Schmidt, K., 1981. On the rotation of Central–East-Iran
497 microplate. Neues Jahrbuch für Geologie und Paläontologie Monatshefte 3, 180–192.
498 Dick, H.J.B., Bullen, T., 1984. Chromian spinel as a petrogenetic indicator in abyssal and
499 alpine-type peridotites and spatially associated lavas. Contributions to Mineralogy and
500 Petrology 86, 54–76.
501 Dickey, J.S., 1975. A hypothesis of origin for podiform chromite deposits. Geochimica et
502 Cosmochimica Acta 39, 1061–1074.
503 Gaetani, M., Angiolini, L., Ueno, K., Nicora, A., Stephenson, M.H., Sciunnach, D., Rettori,
504 R., Price, G.D., Sabouri, J., 2009. Pennsylvanian–Early Triassic stratigraphy in the Alborz
505 Mountains (Iran). In: Brunet, M.F., Wilmsen, M., Granath, J.W. (Eds.), South Caspian to
506 Central Iran Basins. Geological Society London, Special Publication 312, pp. 79–128.
507 Kamenetsky, V.S., Crawford, A.J., Meffre, S., 2001. Factors controlling chemistry of
508 magmatic spinel; an empirical study of associated olivine, Cr-spinel and melt inclusions
509 from primitive rocks. Journal of Petrology 42, 655–671.
510 Lužar-Oberiter, B., Mikes, T., von Eynatten, H., Babić, L., 2009. Ophiolitic detritus in
511 Cretaceous clastic formations of the Dinarides (NW Croatia): evidence from Cr-spinel
512 chemistry. International Journal of Earth Sciences 98, 1097–1108.
513 Mattei, M., Cifelli, F., Muttoni, G., Zanchi, A., Berra, F., Mossavvari, F., Eshraghi, S.A.,
514 2012. Neogene block-rotation in Central Iran: evidence from paleomagnetic data.
515 Geological Society of America Bulletin 124, 943–956.

516 Mattei, M., Cifelli, F., Muttoni, M., Rashid, H., 2015. Post-Cimmerian (Jurassic-Cenozoic)
517 paleogeography and vertical axis tectonic rotations of Central Iran and the Alborz
518 Mountains. Journal of Asian Earth Sciences 102, 92–101.
519 Miall, A.D., 2006. The geology of fluvial deposits. Sedimentary facies, basin analysis, and
520 petroleum geology. Springer, Berlin, 582 pp.
521 Morton, A.C., Hallsworth, C.R., 1999. Processes controlling the composition of heavy
522 mineral assemblages in sandstones. Sedimentary Geology 124, 3–29.
523 Mosier, D.L., Singer, D.A., Moring, B.C., Galloway, J.P., 2012. Podiform chromite deposits–
524 database and grade and tonnage models. USGS Scientific Investigation Report 5157, 45
525 pp.
526 Nogole-Sadat, M.A.A., 1993. Tectonic map of Iran, Treatise on the geology of Iran.
527 Geological Survey of Iran.
528 Nosouhian, N., Torabi, G., Arai, S., 2014a. Metapicrites of the Bayazeh Ophiolite (Central
529 Iran), a trace of Paleo-Tethys subduction-related mantle metasomatism. Neues Jahrbuch
530 für Geologie und Paläontologie Abhandlungen 271, 1–19.
531 Nosouhian, N., Torabi, G., Arai, S., 2014b. Chromian spinels in the Bayazeh serpentinite
532 (Central Iran); implications for their petrogenesis and metamorphism. Goldschmidt
533 Abstracts 2014, 1829.
534 Ogg, J.G., Ogg, G.M., Gradstein, F.M., 2016. Triassic. In: Ogg, J.G., Ogg, G.M., Gradstein,
535 F.M. (Eds.), A Concise Geologic Time Scale, Elsevier, Amsterdam, pp. 133–149.
536 Pagé, P., Barnes, S.J., 2009. Using trace elements in chromites to constrain the origion of
537 podiform chromitites in the Thetford mines ophiolite, Québec, Canada. Economic
538 Geology 104, 997–1018.
539 Pober, E., Faupl, P., 1988. The chemistry of detrital chromian spinels and its implications for
540 the geodynamic evolution of the Eastern Alps. Geologische Rundschau 77, 641–670.

541 Robinson, P.T., Zhou, M.F., Malpas, J., Bai, W.J., 1997. Podiform chromitites: Their
542 composition, origin and environment of formation. Episodes 20, 247–252.
543 Shafaii Moghadam, H., Stern, R.J., 2014. Ophiolites of Iran: Keys to understanding the
544 tectonic evolution of SW Asia: (I) Paleozoic ophiolites. Journal of Asian Earth Sciences
545 91, 19–38.
546 Shafaii Moghadam, H., Li, X.-H., Ling, X.-X., Stern, R.J., Khedr, M.Z., Chiaradia, M.,
547 Ghorbani, G., Arai, S., Tamura, A., 2015. Devonian to Permian evolution of the Paleo-
548 Tethys Ocean: new evidence from U–Pb zircon dating and Sr–Nd–Pb isotopes of the
549 Darrehanjir–Mashhad "ophiolites", NE Iran. Gondwana Research 28, 781–799.
550 Sharkovski, M., Susov, M., Krivyakin, B., 1984. Geology of the Anarak area (Central Iran).
551 Explanatory Text of the Anarak Quadrangle Map 1:250000. Geological Survey of Iran,
552 V/O Tecnoexport USSR Ministry of Geology, Reports 19.
553 Soffel, H.C., Förster, H.G., 1984. Polar Wander Path of the Central-East-Iran Microplate
554 including new results. Neues Jahrbuch für Geologie und Paläontologie Abhandlungen
555 168, 165–172.
556 Soffel, H.C., Davoudzadeh, M., Rolf, C., Schmidt, S., 1996. New palaeomagnetic data from
557 Central Iran and a Triassic palaeoreconstruction. Geologische Rundschau 85, 293–302.
558 Stöcklin, J., 1968. Structural history and tectonics of Iran: A review. American Association of
559 Petroleum Geologists Bulletin 52, 1229–1258.
560 Takin, M., 1972. Iranian geology and continental drift in the Middle East. Nature 235, 147–
561 150.
562 Torabi, G., 2011. Late Permian blueschist from Anarak ophiolite (Central Iran, Isfahan
563 province), a mark of multi-suture closure of the Paleo-Tethys ocean. Revista Mexicana de
564 Ciencias Geológicas 28, 544–554.

565 Torabi, G., 2013. Chromitite absence, presence and chemical variety in ophiolites of the
566 Central Iran (Naein, Ashin, Anarak and Jandaq). Neues Jahrbuch für Geologie und
567 Paläontologie Abhandlungen 267, 171–192.
568 Torabi, G., Arai, S., Koepke, J., 2011. Metamorphosed mantle peridotites from Central Iran
569 (Jandaq area, Isfahan province). Neues Jahrbuch für Geologie und Paläontologie
570 Abhandlungen 261, 129–150.
571 Tozer, E.T., 1972. Triassic ammonoids and *Daonella* from the Nakhlak Group, Anarak
572 region, Central Iran. Geological Survey of Iran, Report 28, 29–69.
573 Vaziri, S.H., 2001. The Triassic Nakhlak Group, an exotic succession in Central Iran. In:
574 Akinci, Ö.T., Görmüş, M., Kuşçu, M., Karagüzel, R., Bozcu, M. (Eds.), Proceedings of
575 the 4th International Symposium on Eastern Mediterranean Geology, Isparta, Turkey, pp.
576 53–68.
577 Vaziri, S.H., Fürsich, F.T., 2007. Middle to Upper Triassic deep-water trace fossils from the
578 Ashin Formation, Nakhlak Area, Central Iran. Journal of Sciences, Islamic Republic of
579 Iran 18, 263–268.
580 Vaziri, S.H., 2012. Geological map of Iran, Nakhlak mine, 1:25,000. Geological Survey and
581 Mineral Exploration of Iran.
582 Zanchi, A., Zanchetta, S., Berra, F., Mattei, M., Garzanti, E., Molyneux, S., Nawab, A.,
583 Sabouri, J., 2009a. The Eo-Cimmerian (Late? Triassic) orogeny in north Iran. In: Brunet
584 MF, Wilmsen M, Granath JW (eds.) South Caspian to Central Iran Basins. Geological
585 Society London, Special Publications 312, pp. 31–55.
586 Zanchi, A., Zanchetta, S., Garzanti, E., Balini, M., Berra, F., Mattei, M., Muttoni, G., 2009b
587 The Cimmerian evolution of the Nakhlak-Anarak area, Central Iran, and its bearing for the
588 reconstruction of the history of the Eurasian margin. In: Brunet, M.F., Wilmsen, M.,
589 Granath, J.W. (Eds.), South Caspian to Central Iran Basins. Geological Society London,
590 Special Publications 312, pp. 261–286.

591 Zanchi, A., Malaspina, N., Zanchetta, S., Berra, F., Benciolini, L., Bergomi, M., Cavallo, A.,
592 Javadi, H.R., Kouhpeyma, M., 2015. The Cimmerian accretionary wedge of Anarak,
593 Central Iran. Journal of Asian Earth Sciences 102, 45–72.
594 Zhou, M.F., Robinson, P.T., 1994. High-Cr and high-Al podiform chromitites, western China:
595 Relationship to partial melting and melt/rock relation in the upper mantle. International
596 Geology Review 7, 678–686.
597 Zhou, M.F., Robinson, P.T., Su, B.X., Gao, J.F., Li, J.W., Yang, J.S., Malpas, J., 2014.
598 Compositions of chromite, associated minerals, and parental magmas of podiform
599 chromite deposits: The role of slab contamination of asthenospheric melts in
600 suprasubduction zone environments. Gondwana Research 26, 262–283.
601
602 **Tables**
603
604 Table 1. Representative EPMA major element oxide analyses for detrital Cr-spinel grains
605 from the Triassic Nakhlak Group of Central Iran.
606
607 **Figure captions**
608
609
610 Figure 1. (a) Iranian major structural units and adjacent areas. Compiled and simplified after
611 Stöcklin (1974), Berberian and King (1981), Angiolini et al. (2007), Bagheri and Stampfli
612 (2008), Kalvoda and Bábek (2010) and Zanchi et al. (2015). CEIM: Central-East Iranian
613 Microcontinent; GKF: Great Kavir Fault; NBF: Naiband Fault. Paleozoic ophiolites in
614 northern Iran: TA = Takab, RS = Rasht, SC = south Caspian Sea basin, AG = Aghdarband,
615 MS = Mashhad. Paleozoic ophiolites in central Iran: An = Anarak, Jn = Jandaq, By =
616 Bayazeh, Pb = Posht-e-Badam. (b) Geological map of the Nakhlak Mountain (redrawn from

Vaziri, 2012) showing the Alam, Baqoroq, and Ashin formations. The studied sections are illustrated by black solid lines. The sample positions are indicated by symbols (see Fig. 1c for details). The location of the Nakhlak mine and the way to the Anarak town are also shown. (c) A simplified log showing stratigraphy of the Nakhlak Group, main lithologies, and sample positions.

Figure 2. (a) Wide view of the Alam Formation and the beginning of the Baqoroq Formation. The Alam Formation is a colorful sequence of fossiliferous limestone and siliciclastic turbidites. The Baqoroq Formation is red mainly conglomeratic sequence. (b) Outcrop of the Alam Formation. The exposure shows the alternation of cm-thick turbidite sandstone lobes (dark color thick to medium-bedded sandstone packages) and calcareous shaly intervals (gray). The inset photo shows a close-up view. (c) Wide view of the red Baqoroq Formation conglomerate. The Alam Formation is also visible. (d) A massive conglomeratic bed from the Baqoroq Formation with the components being in size of cobbles and boulders. (e) A close up view from the Baqoroq Formation outcrop showing chiefly schist (M) and ooid grainstone (L) pebbles. (f) Greenish-gray mostly calcareous shale beds outcrop from the upper parts of the Asin Formation. Backpack (encircled) for scale. The inset photo shows a close up of crinoid bed. (g) Outcrop view of the distal turbiditic sequence of dark thin sandstone beds and medium-bedded greenish-gray shale. The inset photos show trace fossil (left side) and a huge septarian nodule (right side). White arrows in photographs show stratigraphic younging direction.

Figure 3. (a) Photomicrograph from a feldspatholithic sandstone of the Alam Formation. Fresh tabular feldspar grains are noticeable in the centre of the image. The interstitial grains are mainly pseudo-matrix formed by compaction of unstable volcanic detritus. (b) Lathwork

643 and vitric volcanic lithic clast in volcanolithic sandstone from the Alam Formation. The
644 matrix and some feldspar grains are replaced by calcite. (c) Volcanolithic sandstone from the
645 lower part of the Baqoroq Formation. (d) Increase of the abundance of metamorphic clasts in
646 a sandstone from the upper part of the Baqoroq Formation. (e) Polymictic conglomerate
647 includes a gravel of ooid grainstone, which is very common throughout the Baqoroq
648 Formation. (f) Feldspatholithic sandstone from the Ashin Formation. Pl = plagioclase, Kfs =
649 potassium feldspar, Qz = quartz, Lv = volcanic lithic fragment, Lsm = metamorphic lithic
650 fragment, Ls = sedimentary lithic fragment, C = carbonate cementation and/or replacement,
651 C-F = Crinoid fragment. All photomicrographs have been taken in cross-polarized light.
652
653
654 Figure 4. The chemical composition of detrital Cr-spinel grains from the Triassic Nakhlak
655 Group of Central Iran. (a–c) Ternary plots of the major trivalent cations in Cr-spinels (after
656 Cookenboo et al., 1997). Colourful diamonds are values from the detrital Cr-spinel grains of
657 this study. For comparison, light gray fill represents spinel composition from Alaskan-type
658 peridotites. The solid line denotes field for Cr-spinels of mantle melting origin, including
659 ultramafic xenoliths, abyssal dunites, spinel and plagioclase peridotites, and Alpine-type
660 peridotites. Stippled field shows a compositional range of spinels from stratiform intrusions
661 derived by fractional crystallization; (d–f) Cr# vs. Mg# plots showing compositional fields of
662 spinels from the rock types constituting ophiolite suites (after Pober and Faupl, 1988).
663
664
665 Figure 5. The chemical composition of detrital Cr-spinel grains from the Triassic Nakhlak
666 Group of Central Iran. Discrimination between volcanic and mantle spinels using Fe^{2+}/Fe^{3+}
667 vs. Al_2O_3 (a–c) and TiO_2 vs. Al_2O_3 (d–f) compositional relationships (after Kamenetsky et al.,
668 2001). MORB – mid-oceanic ridge basalt, OIB – ocean-island basalt, LIP – large igneous

province, ARC – island-arc magmas, SSZ – -supra-subduction zone. Legend for sample symbols is the same as in Fig. 4.

Figure 6. The chemical composition of detrital Cr-spinel grains from the Triassic Nakhlak Group of Central Iran. TiO_2 vs. Cr# diagram (fields after Pagé and Barnes, 2009). Legend for sample symbols is the same as in Fig. 4.

Figure 7. Schematic diagrams illustrating the possible tectonic and volcano-sedimentary evolution of the Eurasian active margin during Paleozoic and Early Mesozoic times. Please note that for the Palaeozoic the direction of subduction along the intra-oceanic island arc has not been constrained. For the Early–Middle Triassic we suggest the development of a fore-arc basin related to arc extension leading to rapid subsidence and marine influx. The fossils of the Ashin Formation suggest deposition in a deep-marine environment (e.g., Vaziri and Fürsich, 2007). This extensional setting could be the consequence of north-directed oblique subduction of the Paleo-Tethys oceanic crust leading to the development of transform fault zones and pull-apart basins along the southern Eurasian margin (see also Zanchi et al., 2009b).

Electronic supplementary material

Table S1. Cr-spinel chemical data.

Figure S1. Transmitted light optical photomicrographs of Cr-spinel grains.

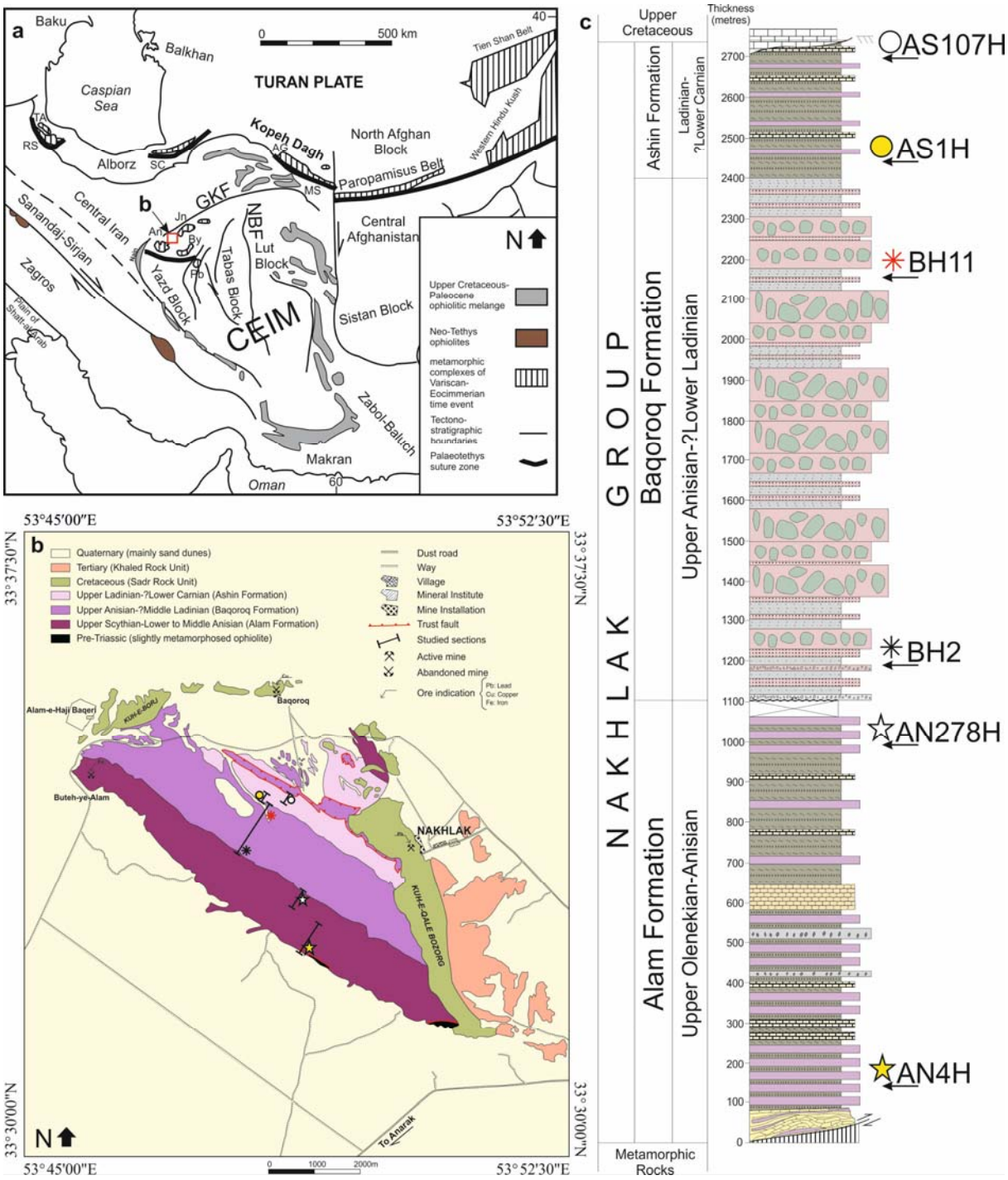
a
Baku
Balkhan
Caspian Sea
TURAN PLATE
0
500 km
40
Tien Shan Belt
Western Hindu Kush
Kopeh Dagh
North Afghan Block
Paropamisus Belt
Alborz
TF
RS
SC
KF
MS
GKF
NBF
b
Jn
An
By
Central Iran
Sanandaj-Sirjan
Zagros
Yazd Block
Tabas Block
Lut Block
Central Afghanistan
Sistan Block
CEIM
Zabol-Baluch
Makran
Oman
60
N
Upper Cretaceous-Paleocene ophiolitic melange
Neo-Tethys ophiolites
metamorphic complexes of Variscan-Eocimmerian time event
Tectono-stratigraphic boundaries
Palaeotethys suture zone
53°45'00"E
53°52'30"E
33°37'30"N
33°30'00"N
Quaternary (mainly sand dunes)
Tertiary (Khaled Rock Unit)
Cretaceous (Sadr Rock Unit)
Upper Ladinian-?Lower Carnian (Ashin Formation)
Upper Anisian-?Middle Ladinian (Baqoroq Formation)
Upper Scythian-Lower to Middle Anisian (Alam Formation)
Pre-Triassic (slightly metamorphosed ophiolite)
Dust road
Way
Village
Mineral Institute
Mine Installation
Trust fault
Studied sections
Active mine
Abandoned mine
Ore indication
Pb: Lead
Cu: Copper
Fe: Iron
Alam-e-Haji Baqeri
KUH-E-BORJ
Baqoroq
Buteh-ye-Alam
NAKHLAK
KUH-E-QALE BOZORG
To Anarak
0
1000
2000m
c
Upper Cretaceous
Ashin Formation
Ladinian-?Lower Carnian
Baqoroq Formation
Upper Anisian-?Lower Ladinian
NAKHLAK GROUP
Alam Formation
Upper Olenekian-Anisian
Metamorphic Rocks
Thickness (metres)
AS107H
AS1H
BH11
BH2
AN278H
AN4H

Fig. 1

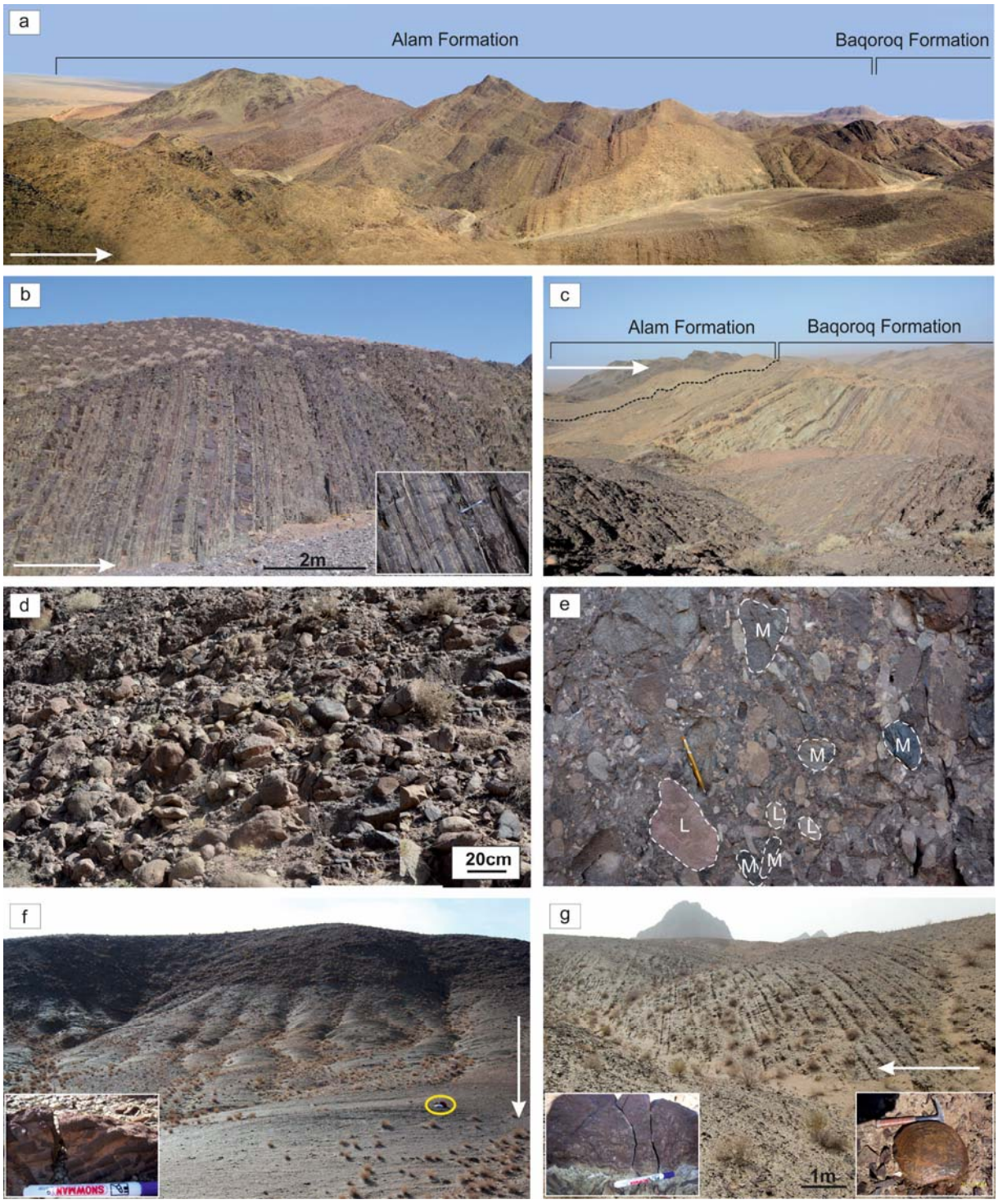
a
Alam Formation
Baqoroq Formation
b
2m
c
Alam Formation
Baqoroq Formation
d
20cm
e
M
M
M
L
L
L
M
M
f
g
1m

Fig. 2

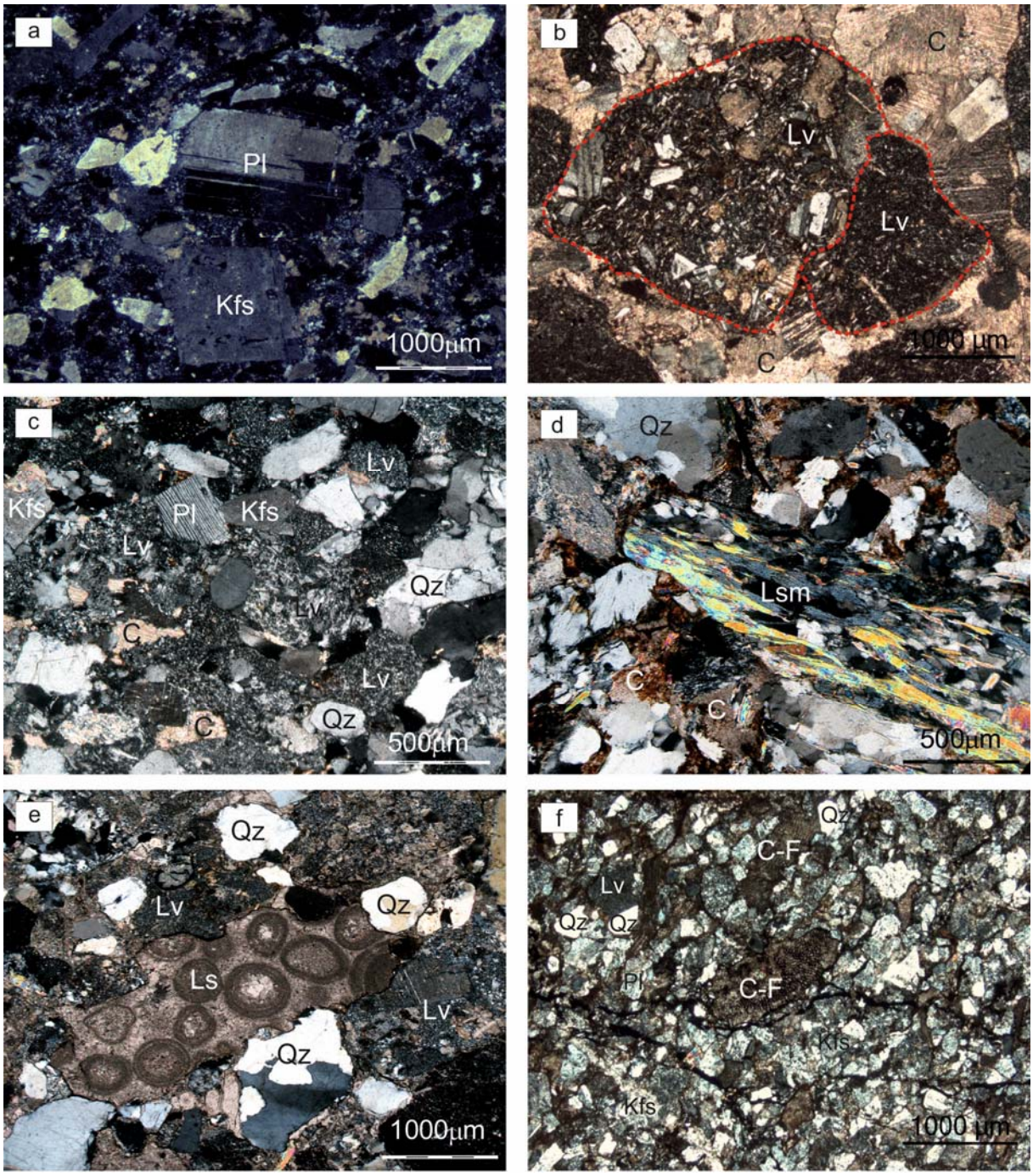
a
Pl
Kfs
1000μm
b
C
Lv
Lv
C
1000 μm
c
Kfs
Pl
Kfs
Lv
Lv
Qz
Lv
C
Lv
C
Qz
500μm
d
Qz
Lsm
C
C
500μm
e
Qz
Lv
Qz
Ls
Lv
Qz
1000μm
f
Qz
C-F
Lv
Qz
Qz
Pl
C-F
Kfs
Kfs
1000 μm

Fig. 3

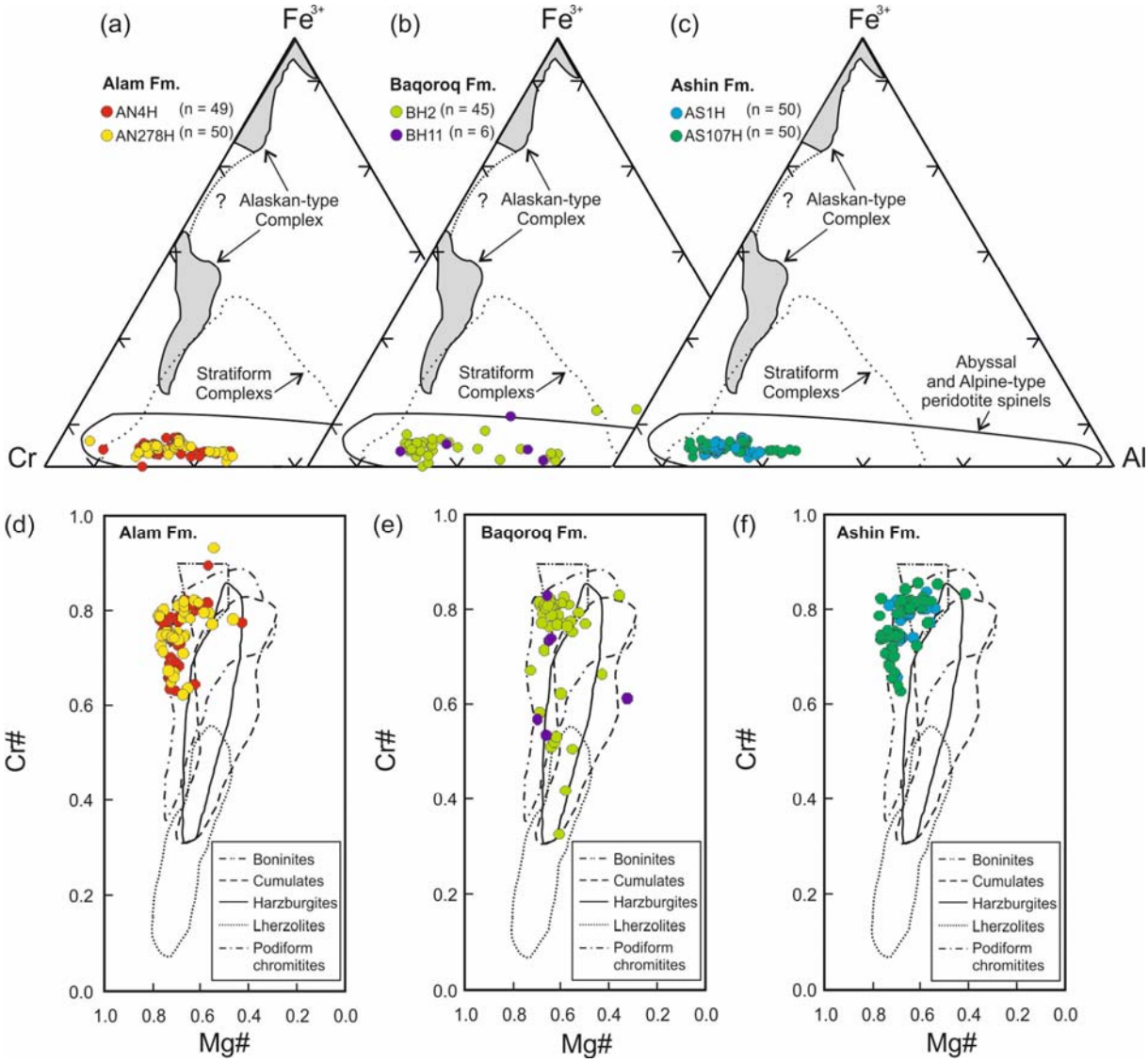
(a)
Fe3+
Alam Fm.
AN4H (n = 49)
AN278H (n = 50)
? Alaskan-type Complex
Stratiform Complexs
Cr
(b)
Fe3+
Baqoroq Fm.
BH2 (n = 45)
BH11 (n = 6)
? Alaskan-type Complex
Stratiform Complexs
(c)
Fe3+
Ashin Fm.
AS1H (n = 50)
AS107H (n = 50)
? Alaskan-type Complex
Stratiform Complexs
Abyssal and Alpine-type peridotite spinels
Al
(d)
Alam Fm.
(e)
Baqoroq Fm.
(f)
Ashin Fm.
Cr#
Mg#
1.0
0.8
0.6
0.4
0.2
0.0
Boninites
Cumulates
Harzburgites
Lherzolites
Podiform chromitites

Fig. 4

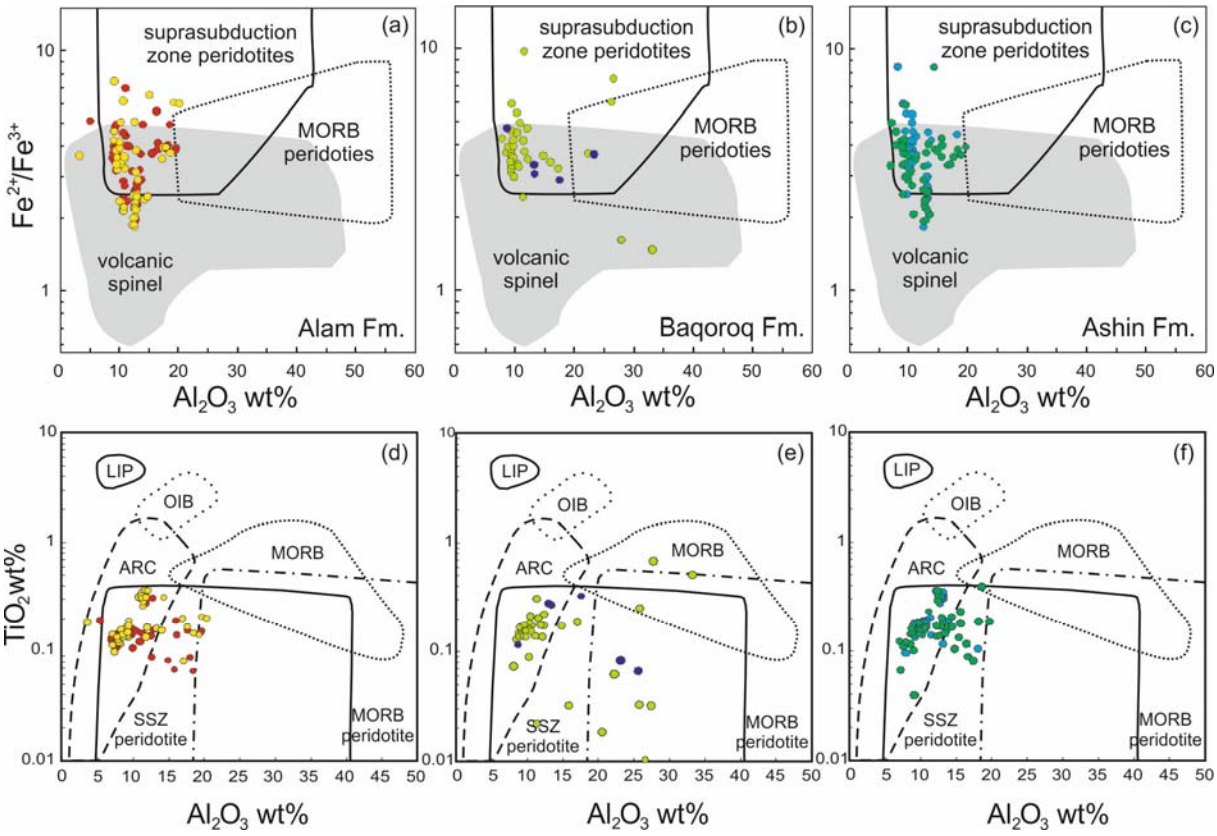
(a)
(b)
(c)
suprasubduction zone peridotites
MORB peridoties
volcanic spinel
Alam Fm.
Baqoroq Fm.
Ashin Fm.
Fe2+/Fe3+
Al2O3 wt%
(d)
(e)
(f)
LIP
OIB
ARC
MORB
SSZ peridotite
MORB peridotite
TiO2wt%

Fig. 5

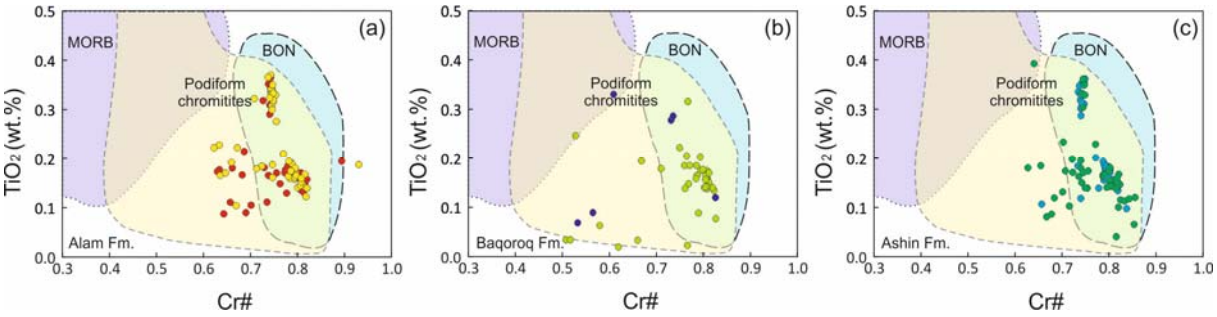
(a)
MORB
BON
Podiform chromitites
Alam Fm.
(b)
MORB
BON
Podiform chromitites
Baqoroq Fm.
(c)
MORB
BON
Podiform chromitites
Ashin Fm.
TiO2 (wt.%)
Cr#
0.0
0.1
0.2
0.3
0.4
0.5
0.3
0.4
0.5
0.6
0.7
0.8
0.9
1.0

Fig. 6

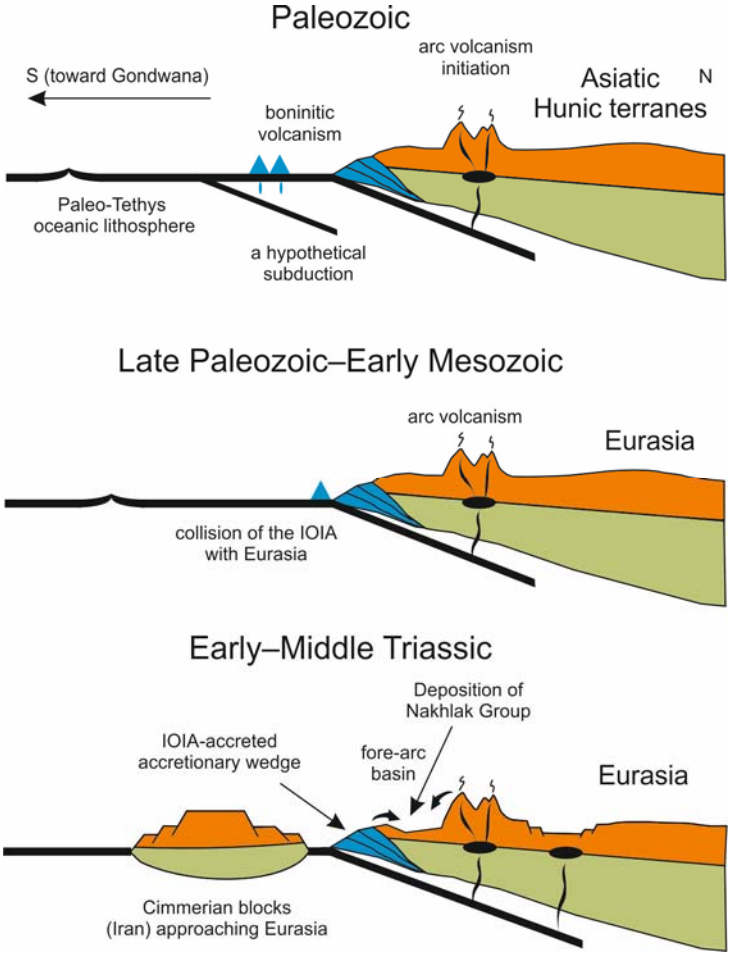
Paleozoic
S (toward Gondwana)
arc volcanism
initiation
Asiatic
Hunic terranes
N
boninitic
volcanism
Paleo-Tethys
oceanic lithosphere
a hypothetical
subduction
Late Paleozoic–Early Mesozoic
arc volcanism
Eurasia
collision of the IOIA
with Eurasia
Early–Middle Triassic
Deposition of
Nakhlak Group
IOIA-accreted
accretionary wedge
fore-arc
basin
Eurasia
Cimmerian blocks
(Iran) approaching Eurasia

Fig. 7